SPAWAR
Systems Center
PACIFIC

TECHNICAL REPORT 3046
September 2016

GENERATION OF QUALITY PULSES FOR CONTROL OF QUBIT/QUANTUM MEMORY SPIN STATES: EXPERIMENTAL AND SIMULATION

Osama Nayfeh
SSC Pacific

Hector Romero
Lance Lerum
NREIP

Mohammed Fahem
SDSU Research Foundation

SSC Pacific
San Diego, CA 92152-5001

SSC Pacific
San Diego, California 92152-5001

K. J. Rothenhaus, CAPT, USN
Commanding Officer

C. A. Keeney
Executive Director

ADMINISTRATIVE INFORMATION

The work described in this report was performed by the Advanced Concepts & Applied Research Branch (Code 71730) of the Advanced Systems and Applied Sciences Division (Code 71700), Space and Naval Warfare Systems Center Pacific (SSC Pacific), San Diego, CA. Further support was provided by student interns from the Naval Research Enterprise Internship Program (NREIP) and the SDSU Research Foundation.

Released by
L. Lemay, Head
Advanced Concepts & Applied Research
Branch

Under authority of
A. D. Ramirez, Head
Advanced Systems and
Applied Sciences Division

ACKNOWLEDGMENTS

We acknowledge funding support of the Office of Naval Research (ONR) In-House Laboratory Initiative for Research managed by Dr. Dave Rees. We acknowledge technical support of Alan Tratumiller. Helpful discussions with David Chao SSC Pacific Code 55360), Son Dinh and Brian Higa (SSC Pacific Code 71730) and Nenad Djapic (SSC Pacific Code 53527). These results are related to the Office of the Secretary of Defense (OSD) Quantum Science and Engineering Program for which these capabilities will be of use.

SB

EXECUTIVE SUMMARY

This technical report presents simulation and experimental hardware development of pulsed modulated microwave/radio-frequency (RF) electronic control circuitry for control of electron/nuclear spin states of qubits/quantum memory applicable to semiconductor, superconductor, ionic, and superconductor-ionic hybrid technologies. As the pulse quality and need for development of single pulses with very high quality will impact directly the coherence time of the qubit/memory, we present as an example the integration of cryogenic superconductor components, including filters and amplifiers to improve the pulse quality and validate the approach. Control of qubits/quantum memory using this technology will be subject of future report.

CONTENTS

Figures

Tables

1. INTRODUCTION

Quantum memory spin states refer in some cases to the combinations of magnetic and nuclear spins of an entangled ensemble or of single spins or photons. These quantum states can be controlled by resonant microwave fields and observed by monitoring the changing time-average photoluminescence intensity. The experiment apparatus for the electronic control of these quantum memory spin states will be discussed in detail and implemented in a laboratory.

2. QUBIT CONTROL

The spin of the nucleus and electrons of an atom are used to encode qubits where NMR (nuclear magnetic resonant) pulses and EPR (electron paramagnetic resonant) pulses are used to perform quantum logic. These two spins encode data of a 2-bit register in the form of |ms,mI>, resulting in four total states that the register can be in. Spin up denotes the 0 state for both electrons and nuclei; however arrows are used to distinguish the two. These four states are $|0, \uparrow\rangle$ $|0, \downarrow\rangle$ $|1, \uparrow\rangle$ $|1 \downarrow\rangle$, see Table 1.

Table 1. The spin of the nucleus and electrons.

Register	Spin Up	Spin Down
Electron Spin: ms	0	1
Nuclear Spin: mI	↑	↓

Electron spins are probed by EPR while monitoring changes in photoluminescence, a procedure known as ODMR (Optically Detected Magnetic Resonance) while nuclear spins are probed by NMR while monitoring changes in photoluminescence, a procedure known as ODNMR (optically detected nuclear magnetic resonance). Both of these procedures require microwave and RF pulses, respectively, at various phase shifts, power, and duration to control the spin. An I/Q mixer is used to generate these microwave and RF pulses with enough efficiency to appropriately execute ODMR and ODNMR spectroscopy.

As mentioned, resonant microwave pulses control these qubits. The applied microwave power determines the rotation rate while the duration of the pulse determines the length of time over which the angle is rotated. The phase of the rotation axis is controlled by the phase of the MW field. There are many variables at play in calculating these factors. Spin density, for example, influences the angular momentum, which relates to the speed of the rotation.

Singular electronic pulses can actually perform qubit spin rotation. However, with current hardware technology impossible to control the MW field strength and the pulse duration with enough accuracy to control the spin states reliably. A rotation angle error arises from the inaccuracy of the pulse width (pulse length error) and/or MW field resonance (off-resonance effect). These errors cause over-rotation and tilted rotational axes respectively.

There have been many proposed methods of suppressing these errors. Of these, the BB1 sequence has promise to be the most effective. One version of the BB1 sequence replaces the single 180˚ rotation with a sequence of three composite pulses. Ideally, the result of an 180x˚ rotation is the same as an 180y˚ and an 180z˚ rotation. These rotations correspond to an electronic transition from |0> to |1>. However, if the resonant frequency or the pulse width is not exact, one will instead have a rotation of $180^\circ \pm \varepsilon$, where ε is the error and is oftentimes quite large.

One can instead perform (ideally) a rotation sequence of 90y˚180x˚90y˚ to achieve the same result (see Figure 1). A sequence of 90y˚± ε, 180x˚± ε, 90y˚± ε will greatly reduce the off-resonant effects that occur in a singular pulse scenario. These different pulses are generated through I/Q modulation.

Figure 2 is a representation of the BB1 sequence given some error. The I-pulses do not perfectly align the electron spin into the π/2 state; however, the correctional Q-pulse reduces the error, allowing the spin of the electron to align closely with the π state. This alignment allows for the inherent error of signals while still ensuring acceptable results. The dark blue line on the Bloch sphere represents the path of the spin of the electron. The red line indicates a successful π rotation given the three pulses.

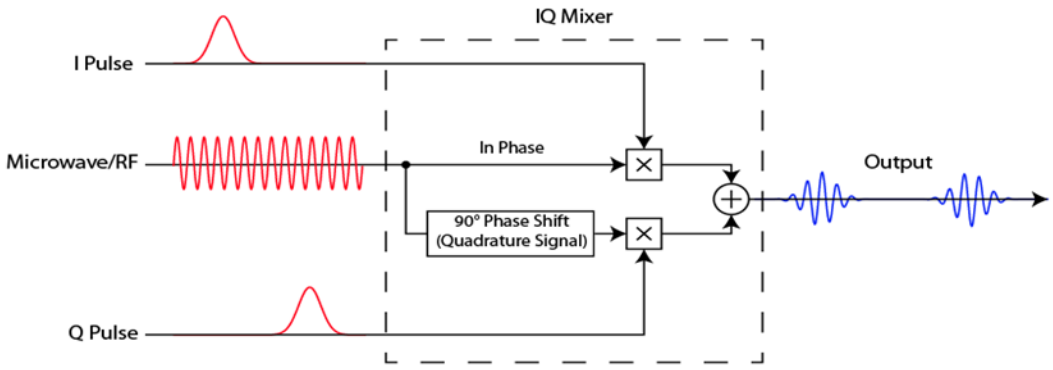

Figure 1. Rotation sequence of 90y˚180 x˚90y˚.

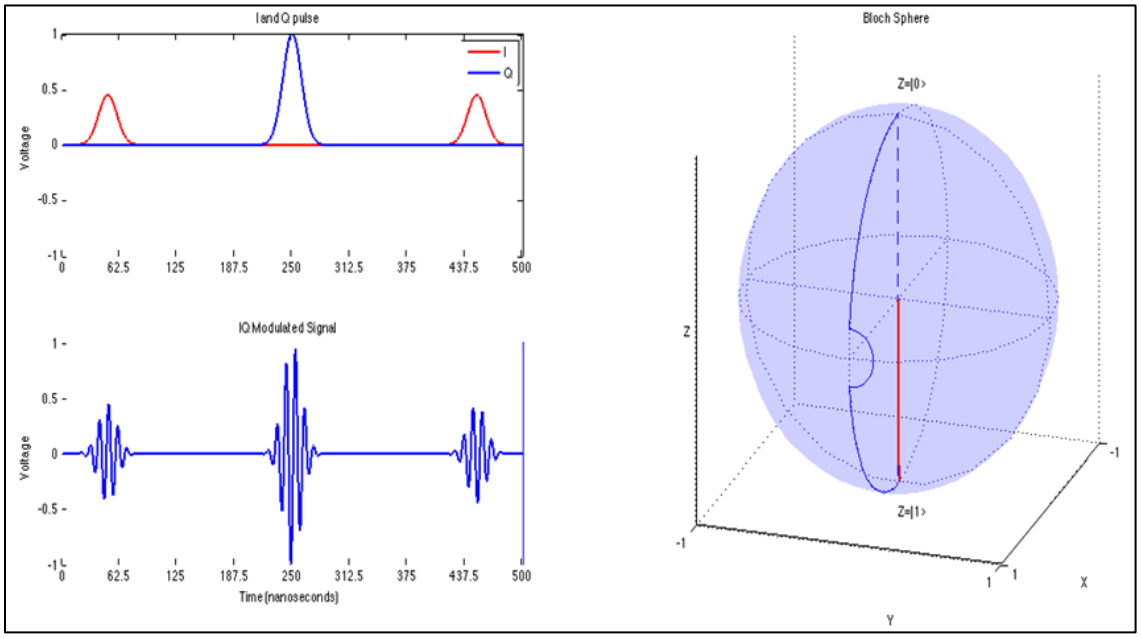

Figure 2. Simulated I/Q pulses demonstrating expected control of the spin flipping and rotation in the Bloch sphere.

3. I/Q MODULATION

The two major components that make up an I/Q mixer are the in-phase modulation (I) and quadrature modulation (Q). The input microwave signal is broken down into an in-phase signal and an identical signal shifted by 90°. We can think of the in-phase signal as a cosine wave and the quadrature signal as a sine wave. The schematic in Figure 3 shows the final output to be of the form and represents amplitude modulation as a function of time.

The two examples show how I-modulation affects the output. Figure 3A shows an example of how a positive "I" wave produces a signal that is completely in phase with the original signal (light blue). Figure 3B shows how a negative "I" wave produces a signal that is 180° out of phase since the original signal is just flipped along the horizontal x-axis. These two examples were produced with =0, therefore, completely ignoring the quadrature signal.

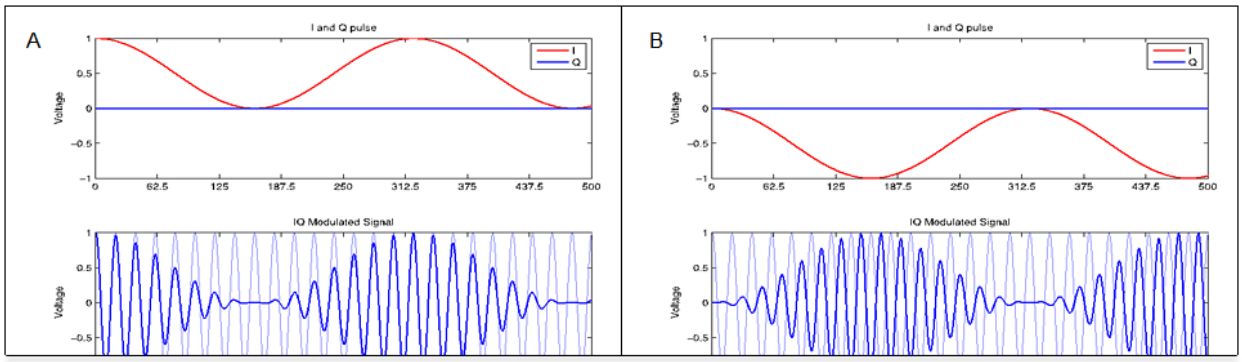

Figure 3. Two examples of I-modulation effects to the output.

Figure 4 shows how an I/Q mixer drives ODMR spectroscopy to control spins of electrons. Five pulses are sent. We will refer to these pulses as pulse 1–5 respectively. Pulse 1 generates an in-phase signal, pulse 2 generates a signal 180° out of phase, pulse 3 generates a signal 90° out of phase, pulse 4 generates a signal 90° out of phase with half amplitude, and pulse 5 generates the same signal as pulse 4. The Bloch spheres represent how each pulse affects the spin of the electron.

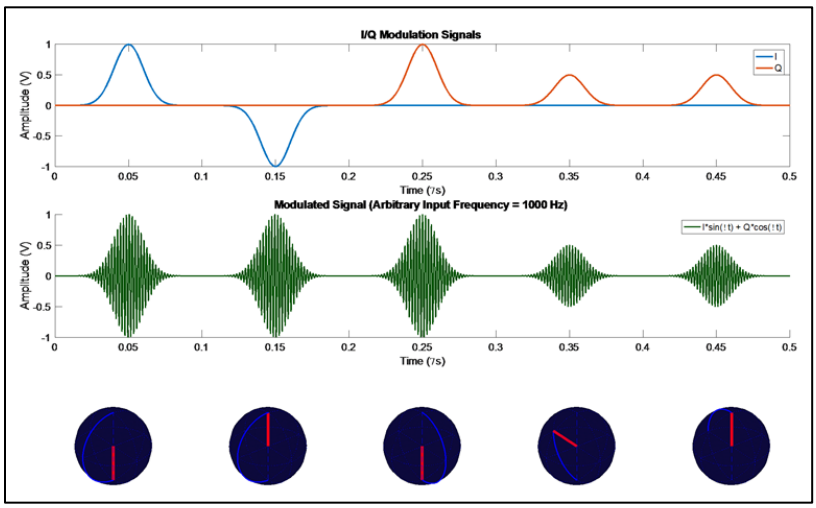

Figure 4. An I/Q mixer drives ODMR spectroscopy to control spins of electrons.

3.1 SIMULATION MODEL USING MATLAB®/SIMULINK

Figure 7 presents the Simulink simulation example of I/Q modulation followed by a switch controlled by a square wave. The I-pulse is an arbitrary example shown in Figure 8, while the Q-pulse is modeled as 0.

4. ELECTRICAL SETUP

The electrical control portion of this experiment starts with the Arbitrary Waveform Generator (AWG). The AWG generates a RF signal for nuclear excitation, Gaussian-shaped I/Q pulses for microwave modulating, and composite rectangular pulses for gate control. Figure 5 shows four signals as the input to the multiplexer, and each signal will be named by their respective select pins as shown.

As called for in the original experiment, the I/Q output pulses from the AWG are inputted into vector signal generators (VSGs). These VSGs provide a local oscillator that is modulated by the I/Q signals. There are two modulated pulsed signals for electron spins for better gate control. Signal 2 generates a pulse that is always at a 90° phase shift, while Signal 1 is always for a more arbitrary phase-shift pulses, which allows for select pins to quickly switch between the two. Signal 3 is generated specifically for nuclear spin manipulation and signal 4 is generated specifically for electron spin initialization.

Paths 1–4 are all connected to high-speed switches that are controlled by the rectangular pulses from the AWG. The outputs of these switches are band-pass filtered and then inputted into a multiplexer. The output of the multiplexer is amplified and then passed into a directional coupler. One output is passed through a schottky diode and then into an oscilloscope. The other signal is sent to a strip-line antenna that controls the qubit.

A potential alternative to the use of two VSGs, which are expensive, is the use of an I/Q mixer. The I/Q mixer could use the MW output of the one VSG as the RF input, and the I and Q from the AWG as modulators, which allows the two modulated signals to have the same local oscillating frequency. The VSG used as the local oscillator has a built in I/Q modulator, so only one additional I/Q mixer would be needed.

ODMR/ODNMR in Figure 5 represent optical detection and optical excitation. This portion of the setup will be described in more detail in the optical setup of the experiment.

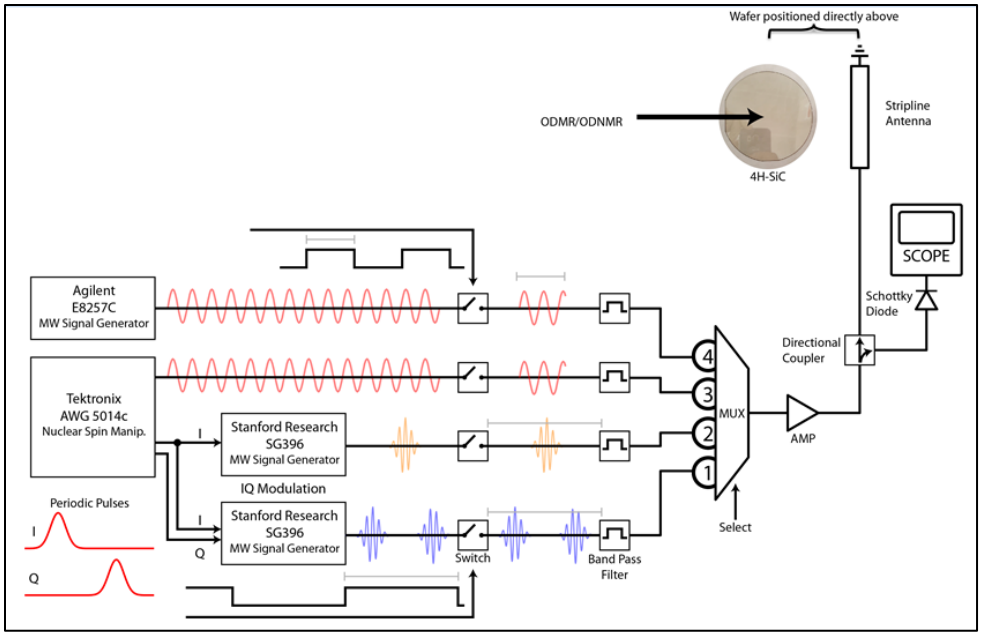

Figure 5. Schematic for electrical setup of qubit control by I/Q modulation.

5. IMPROVING PULSE QUALITY WITH INTEGRATION OF CRYOGENIC AND SUPERCONDUCTING COMPONENTS

Pulse shape, width, power, phase, frequency, and quality are all significant variables to how qubits respond. The most ideal case is the signal generated in a simulation. However, there are limitations to signal generators, filters, amplifiers, and cables, which may result in unfavorable results. These pulses are to be analyzed through various cryogenic and non-cryogenic filters and amplifiers and compared to with the ideal simulation. Figure 6 shows the equipment used that produced the results in this chapter. The first part of this chapter examines five amplifiers.

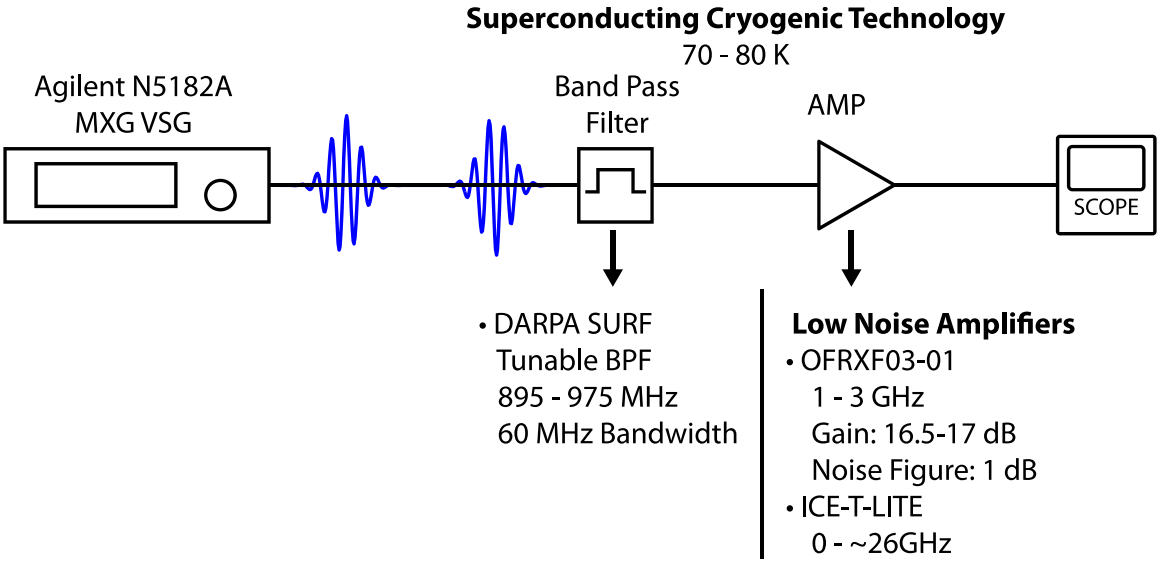

Figure 6. Schematic showing the equipment of interest and how data is collected.

5.1 Cryogenic Low-Noise Amplifiers (LNA)

Figure 7 plots the noise figure and gain for five amplifiers using the Agilent N8975, NFA Series. Two of these amplifiers are superconducting cryogenic amplifiers operating at roughly 80 K. The Hypress ICE-T has the largest operating frequency range, however, the noise figure begins to increase above ~8 GHz, which could be resolved under lower temperatures. Still, the lowest noise figure comes from the OFR Cryo-LNA while also proving ample gain.

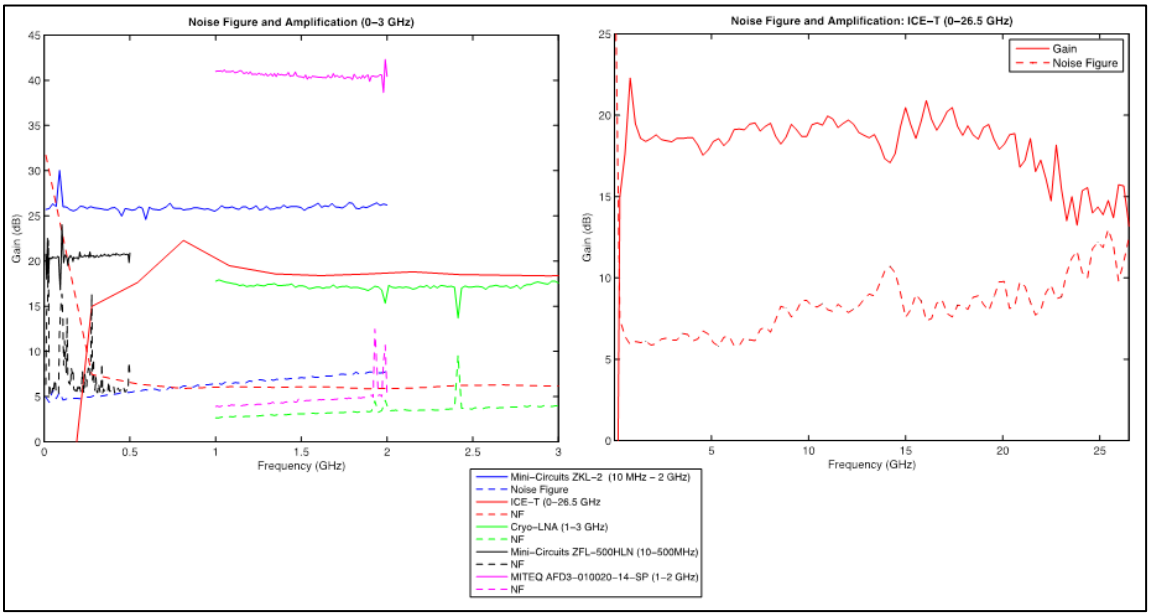

Figure 7. Experimentally measured noise figure and gain for several low-noise amplifiers, including COTF and cryogenically cooled components that achieve lower reduced noise figure while maintaining high gain.

Figure 8 plots the simulation in red and a direct output from the VSG in blue. The VSG alone provides a high-quality pulse train with a 15-MHz carrier frequency. However, the VSG has a limit of 17-dBm power output, which makes amplification a requirement for ODNMR and ODMR.

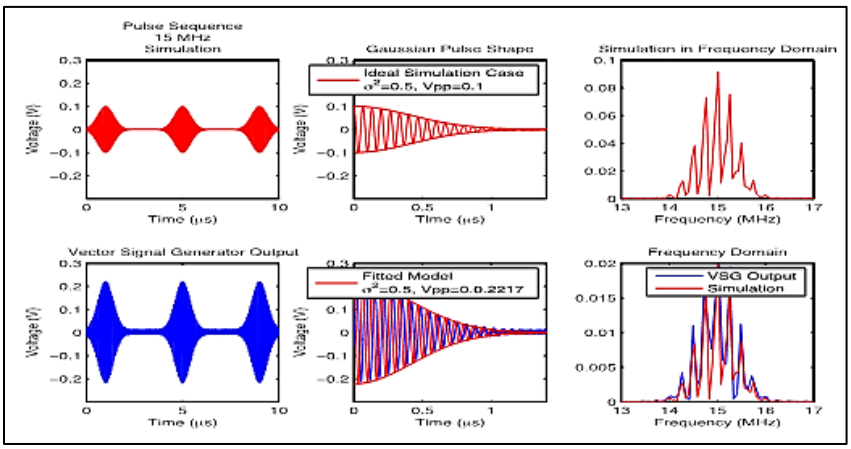

Figure 8. Experimentally measured pulses taken directly from the VSG in time and frequency domain in comparison with an ideal Gaussian envelope pulse carrier of 15 MHz.

Figure 9 plots the results of the Gaussian pulses running through the OFR Cryo-LNA. The plots are comparable. One noticeable effect is the decrease in power as frequency increases; however, this could be adjusted with a preamplifier for the experiment.

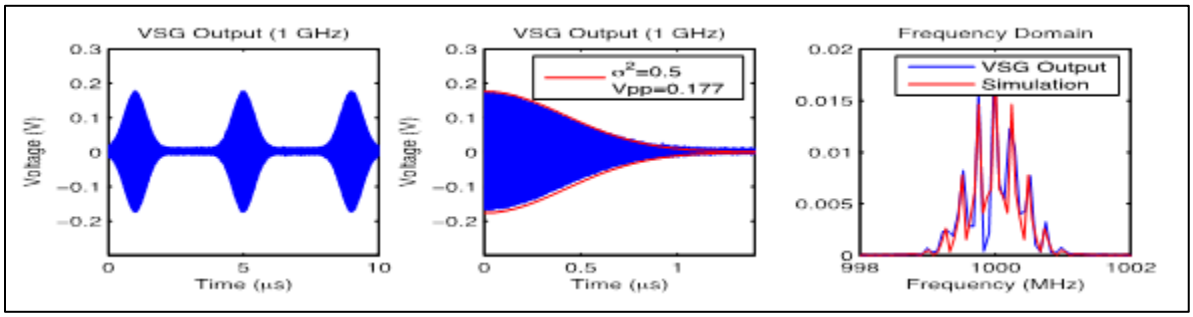

Figure 9. Experimentally measured pulses taken directly from the VSG in time and frequency domain in comparison with an ideal Gaussian envelope pulse carrier of 1 GHz.

Figure 10 experimentally measured pulses in time and frequency domain in comparison with an ideal Gaussian envelope pulse carrier of 1 GHz through a cryogenically cooled low-noise amplifier in comparison with the ideal simulation.

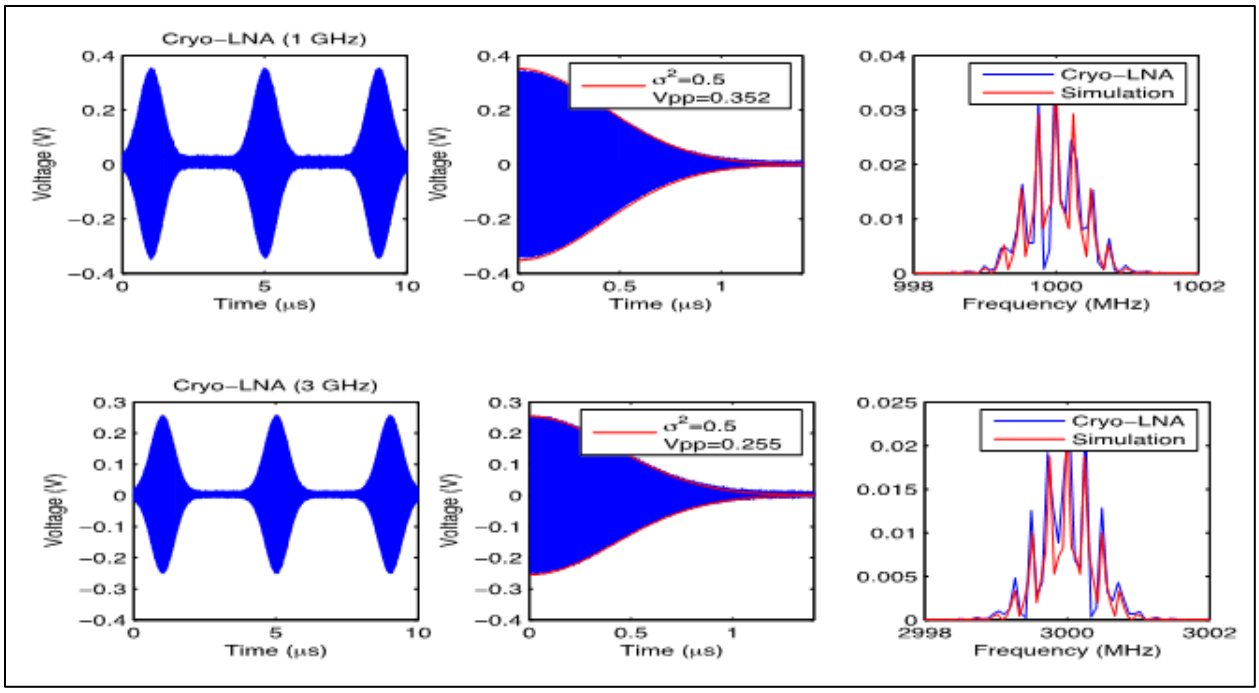

Figure 10. Measured pulses in time and frequency domain in comparison with an ideal Gaussian envelope pulse carrier of 1 GH.

Figure 11 experimentally measured pulses in time and frequency domain in comparison with an ideal Gaussian envelope pulse carrier of 1 GHz through the ICE-T, which shows that the signal has been clipped.

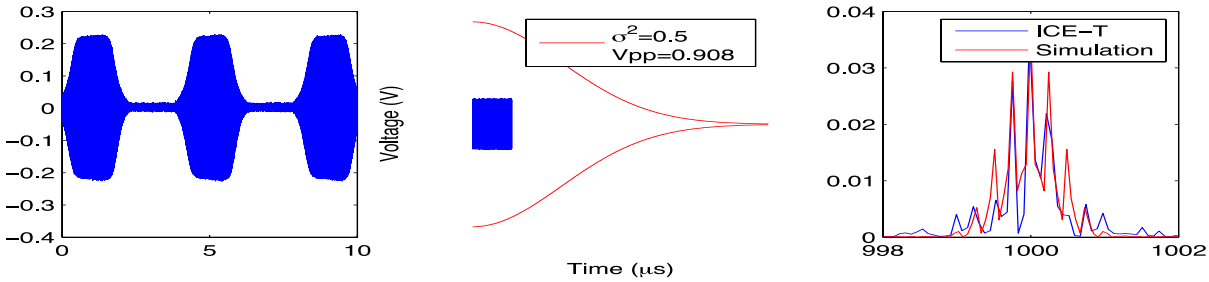

Figure 11. Measured pulses in time and frequency domain in comparison with an ideal Gaussian envelope pulse carrier of 1 GHz through the ICE-T.

Results from three non-cryogenic amplifiers are plotted in Figure 12. Mini-Circuits ZFL-500HLN at the top of the figure best resembles the ideal case, but works in a frequency range that is incompatible with the experiment. The results of amplifying the Gaussian pulse signal from the Mini-Circuits ZKL-1R5 and the MITEQ AFD3 establishes a motivation for improving pulse quality for maximizing lifetime and fidelity of electronic and nuclear spins that define the qubit..

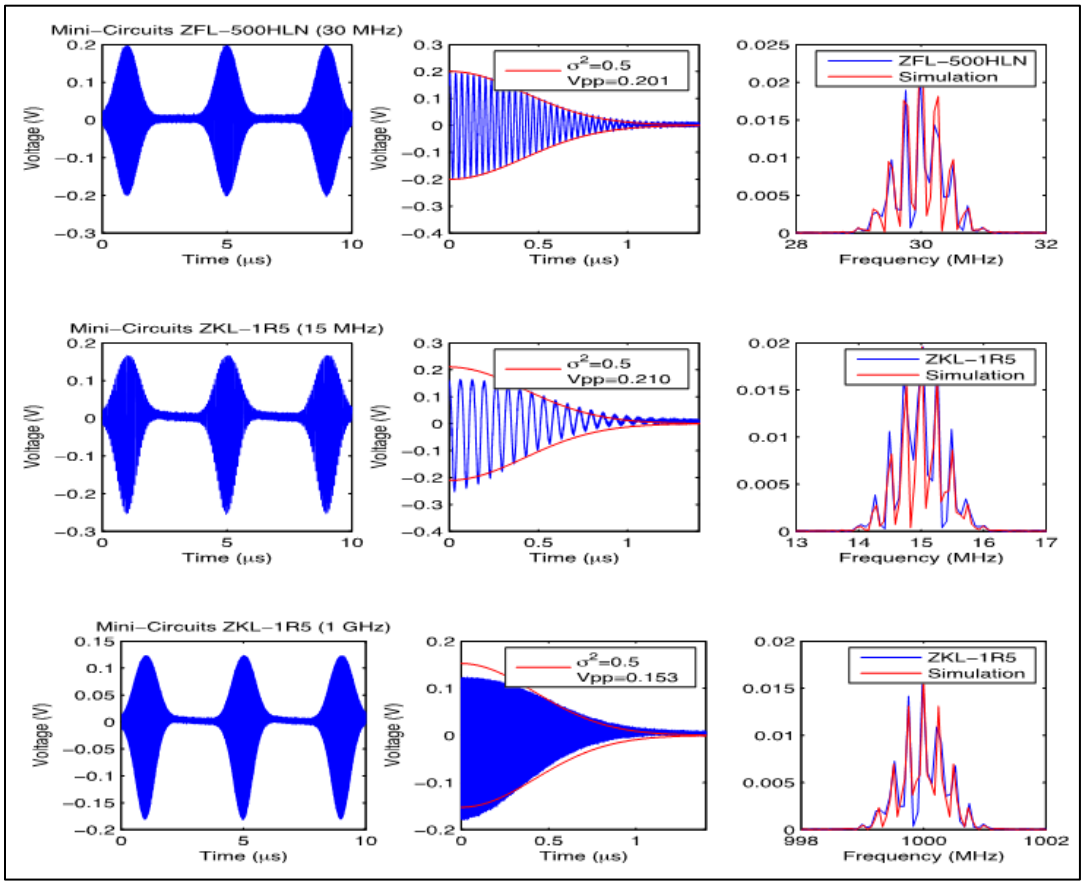

Figure 12. Results from three non-cryogenic amplifiers.

Overall, the amplifier measurements shown in Figure 13 look excellent and resemble the ideal case very well in the frequency domain. Figure 14 examines the noise floor of all amplifiers in the frequency domain from 0–2.5 GHz, given a 1-GHz carrier frequency. The second row of graphs plots the cryogenic amplifiers of a 3-GHz carrier from 0–6.5 GHz.

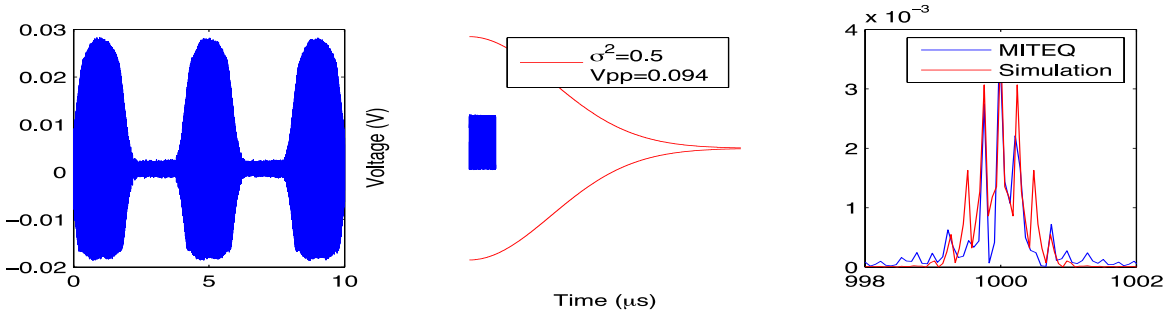

Figure 13. Experimentally measured pulses in time and frequency domain in comparison with an ideal Gaussian envelope through COTF amplifiers showing their limitations at high frequencies. The shape of the Gaussian is generally distorted using these amplifiers.

Figure 14 shows measurements taken in the frequency domain of four amplifiers in comparison with the ideal simulation when all the data is normalized. Although the Cry-LNA (OFR) has the most noise in these frequency regions, it did retain the best pulse shape. It may be possible to further reduce noise given a cryogenic band-pass filter.

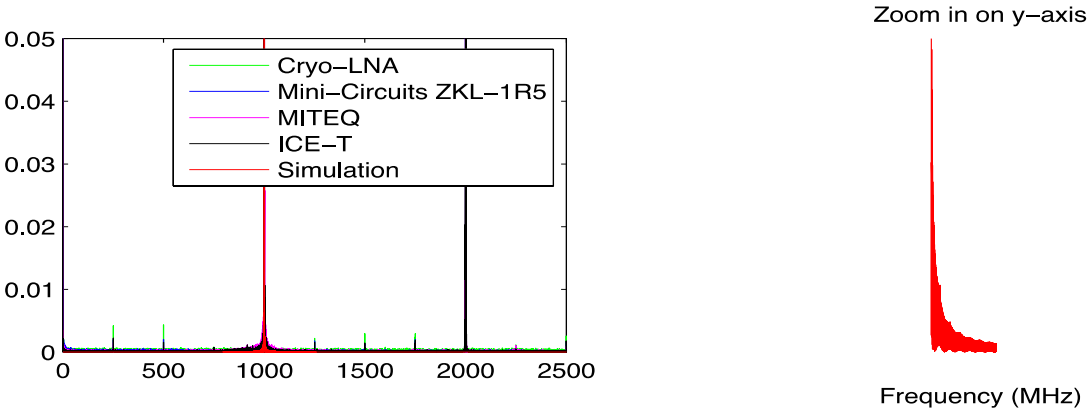

Figure 14. Measurements taken in the frequency domain of four amplifiers in comparison with the ideal simulation when all the data is normalized.

Figure 15 shows measurements taken in the frequency domain of the two cryogenically cooled low-noise amplifiers in comparison with the ideal simulation when all the data is normalized.

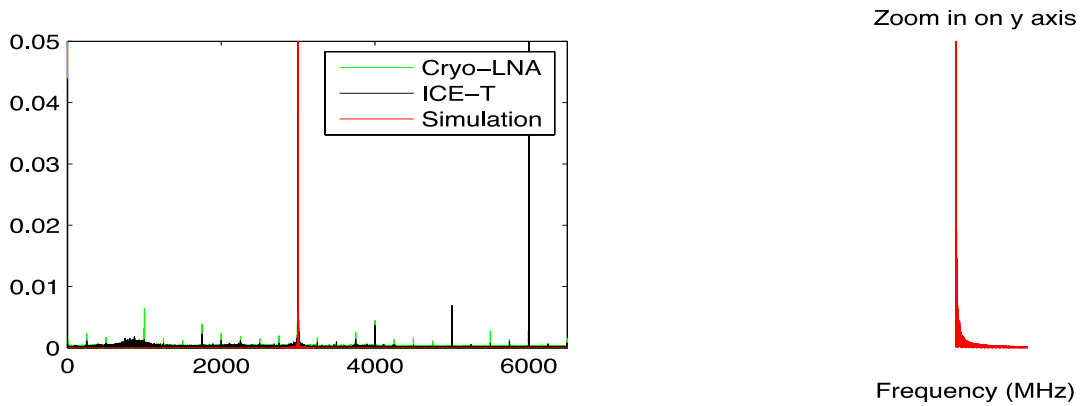

Figure 15. Measurements taken in the frequency domain of the two cryogenically cooled low-noise amplifiers in comparison with the ideal simulation when all the data is normalized.

The plot appears to contradict the noise floor shown in Figure 9 for the OFR Cryo-LNA. It is possible to further improve the OFR-Cryo LNA by adding a band-pass filter. The reasoning behind adding the band-pass filter before the OFR-Cryo LNA is that the current cryogenic band-pass filter in question (DARPA SURF) contains an RF limiter in its configuration to prevent any damage to it from high-power RF signals.

5.2 CRYOGENIC BAND-PASS FILTERS

This section analyzes the block diagram below at different power levels supplied by the VSG. A Gaussian pulse with a 950-MHz carrier frequency is sent at -40, -20, -10, 0, 10 dBm. DARPA SURF is a cryogenic superconducting tunable band-pass filter tuned to 950 MHz with a 60-MHz bandwidth. The signal is then passed to the OFRXF03-01 Cryo-LNA. Figure 16 shows the Gain plot of DARPA SURF tunable band-pass filter tuned to 950 MHz.

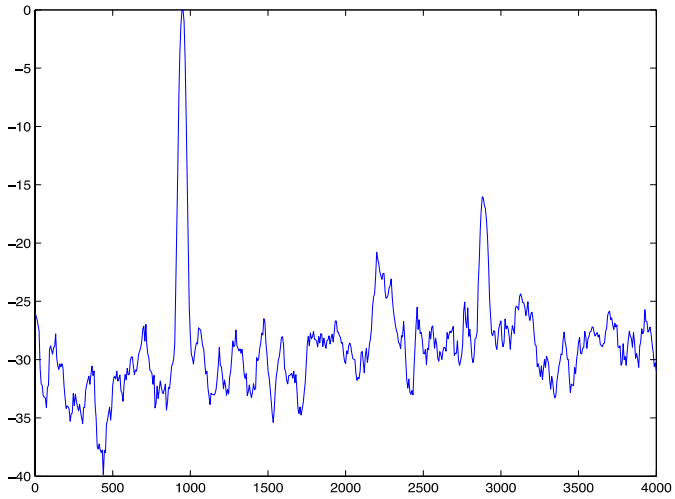

Figure 16. Gain plot of DARPA SURF tunable band-pass filter tuned to 950 MHz.

Figure 17 shows experimental measurements taken with a VSG at -50 dBm comparing results taken directly through the band-pass filter, and through the band-pass filter, followed by an LNA.

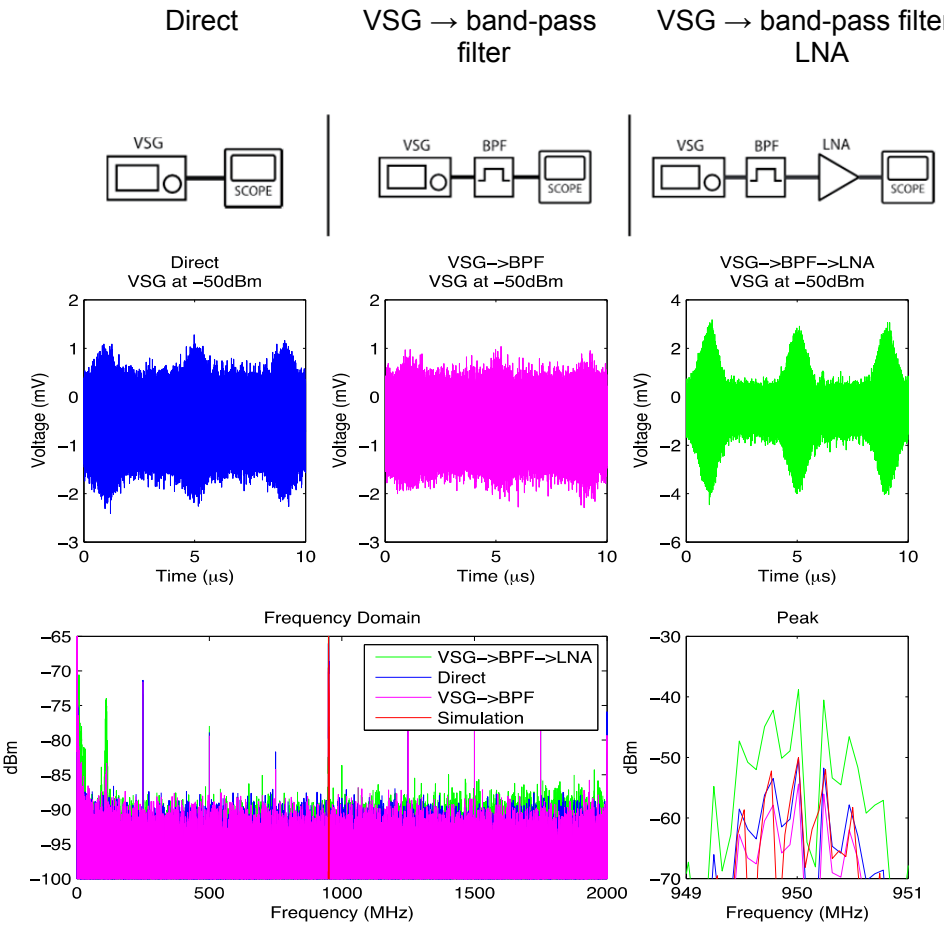

Figure 17. Experimental measurements taken with a VSG at -50 dBm comparing results taken directly through the band-pass filter, and through the band-pass filter, followed by an LNA.

Figure 18 shows experimental measurements taken with a VSG at -40 dBm comparing results taken directly through the band-pass filter, and through the band-pass filter, followed by an LNA.

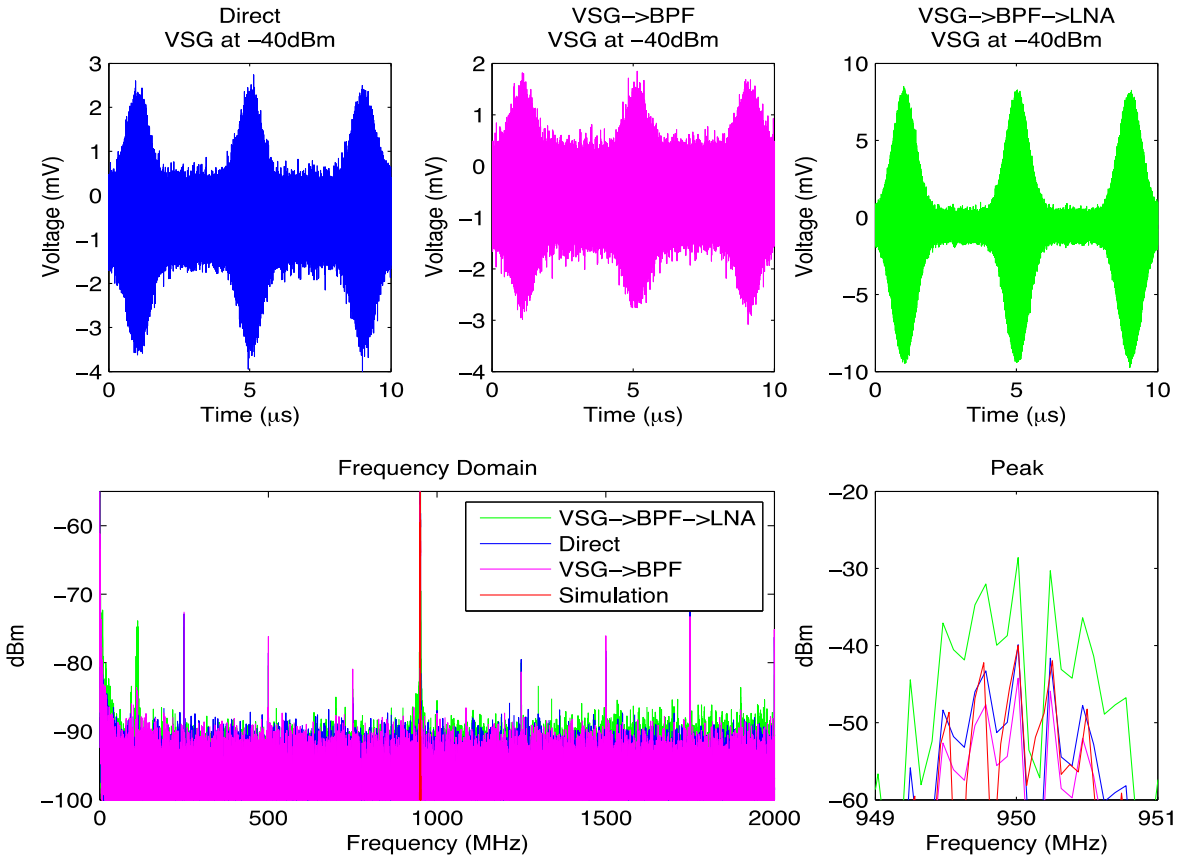

Figure 18. Experimental measurements taken with a VSG at -40 dBm comparing results taken directly through the band-pass filter, and through the band-pass filter, followed by an LNA.

Figure 19 shows experimental measurements taken with a VSG at -30 dBm comparing results taken directly through the band-pass filter, and through the band-pass filter, followed by an LNA.

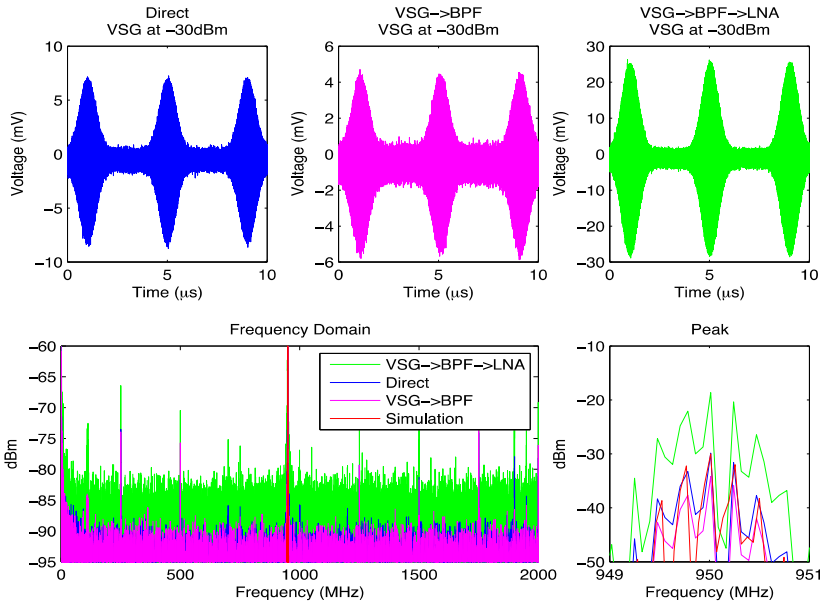

Figure 19. Experimental measurements taken with a VSG at -30 dBm comparing results taken directly through the band-pass filter, and through the band-pass filter, followed by an LNA.

Figure 20 shows experimental measurements taken with a VSG at -20 dBm comparing results taken directly through the band-pass filter, and through the band-pass filter, followed by an LNA. This figure is starting where it shows a decrease in noise when the VSG is sending signals above -20 dBm.

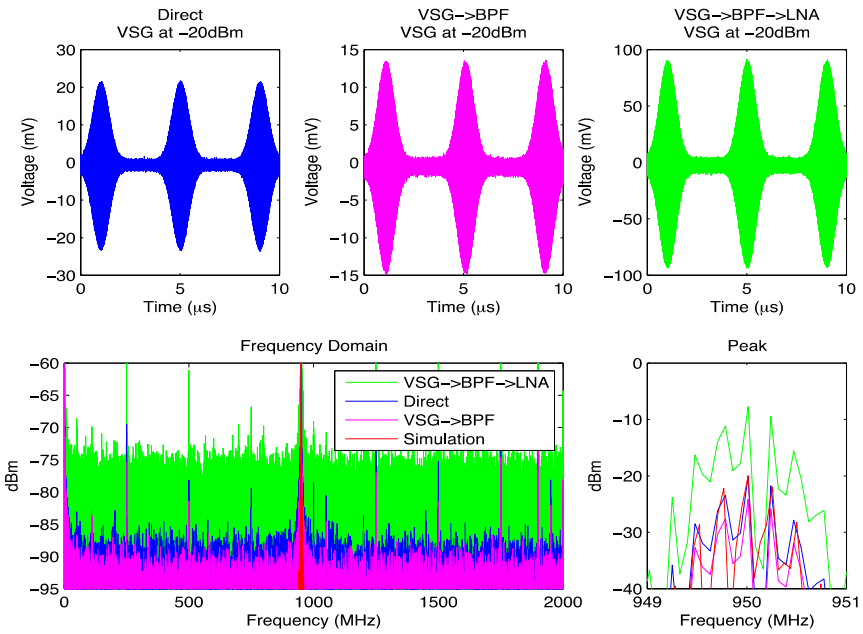

Figure 20. Experimental measurements taken with a VSG at -20 dBm comparing results taken directly through the band-pass filter, and through the band-pass filter, followed by an LNA.

Figure 21. Experimental measurements with a VSG at -10 dBm comparing results taken directly through the band-pass filter, and through the band-pass filter, followed by an LNA. The noise is reduced even more when the VSG is followed by the cryogenic band-pass filter.

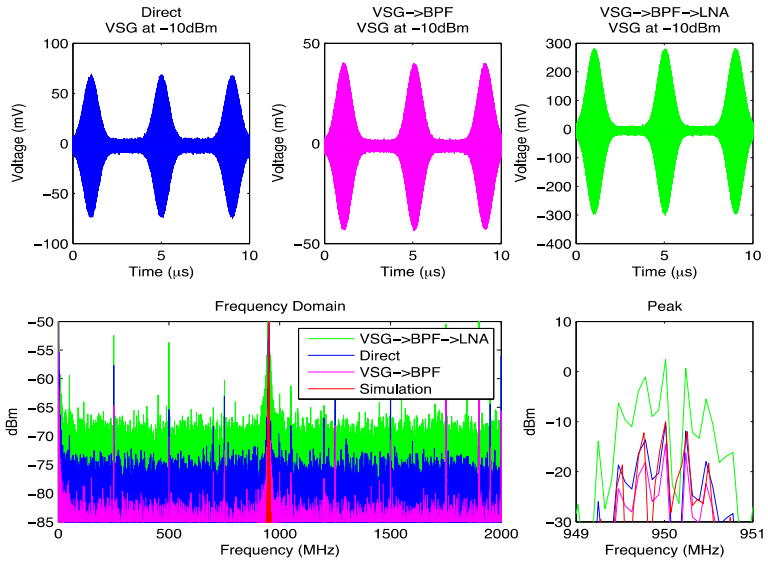

Figure 21. Experimental measurements taken with a VSG at -10 dBm comparing results taken directly through the band-pass filter, and through the band-pass filter, followed by an LNA.

Figure 22 shows experimental measurements taken with a VSG at 0 dBm comparing results taken directly through the band-pass filter, and through the band-pass filter, followed by an LNA. Noise reduction peaks when the VSG outputs power above -10 dBm. At these levels, the band-pass filter is able to reduce the noise floor to, at most, 10 dBm with peak gain reduction of less than 5 dBm.

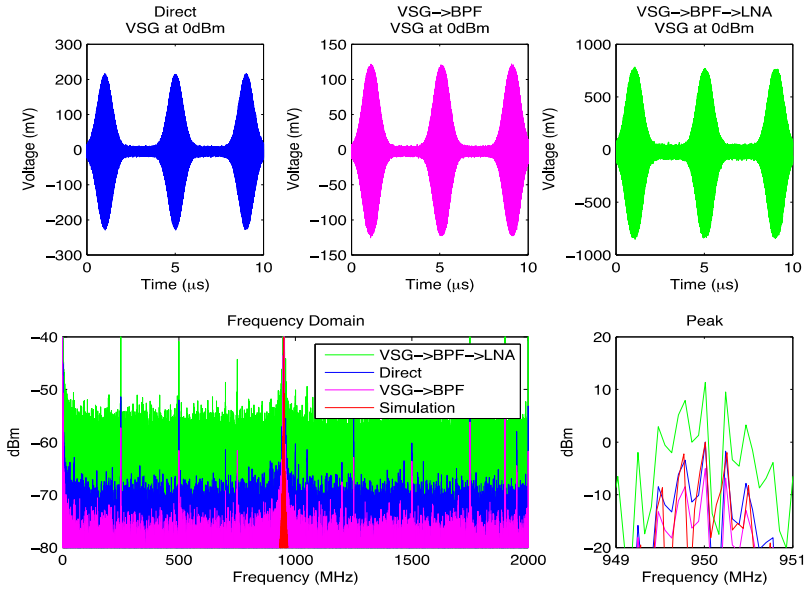

Figure 22. Experimental measurements taken with a VSG at 0 dBm comparing results taken directly through the band-pass filter, and through the band-pass filter, followed by an LNA.

Figure 23 shows experimental measurements taken with a VSG at 10 dBm comparing results taken directly through the band-pass filter, and through the band-pass filter, followed by an LNA. The band-pass filter is equipped with an RF limiter, where its effect can be seen when the VSG operates at more than 10 dBm. The results are no longer practical.

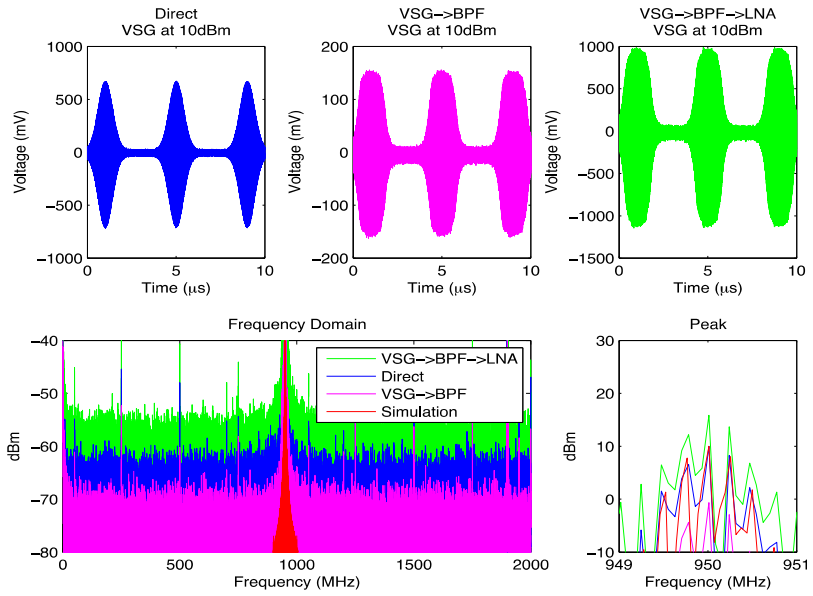

Figure 23. Experimental measurements taken with a VSG at 10 dBm comparing results taken directly through the band-pass filter, and through the band-pass filter, followed by an LNA.

In summary, Figures 17–23 presented plots of the pulses in time and frequency domain when the vector signal generator is operating at different power levels from -50 to 10 dBm in increments of 10 to determine the most optimal operating levels. The proficiency of the band-pass filter begins to increase when the power levels are increased about -20 dBm. Loss in noise is most optimal at -10 and 0 dBm at close to a 10-dBm difference between the direct reading and the VSG to band-pass filter reading, with only a loss of close to 5 dBm at the 950-MHz frequency.

6. BIBLIOGRAPHY

Bladh, K., D. Gunnarsson, E. Hürfeld, S. Devi, C. Kristoffersson, B. Smålander, S. Pehrson, T. Claeson, P. Delsing, and M. Taslakov. 2003 "Comparison of Cryogenic Filters for Use in Single Electronics Experiments," *Review of Scientific Instruments*, vol. 74, no. 3, pp. 1323–1327.

Carter, S. G., Ö. O. Soykal, P. Dev, S. E. Economou, and E. R. Glaser. 2015. "Spin Coherence and Echo Modulation of the Silicon Vacancy in 4 H− SiC at Room Temperature," *Physical Review*, vol. B92, no. 16, pp. 161–202.

Klimov, P, V., A. L. Falk, D. J. Christle, V. V. Dobrovitski, and D. D. Awschalom. 2015 "Quantum Entanglement at Ambient Conditions in a Macroscopic Solid-state Spin Ensemble," *Science Advances*, vol. 1, no. 10, e1501015.

Mallet, F., F. R. Ong, A. Palacios-Laloy, F. Nguyen, P. Bertet, D. Vion, and D. Esteve. 2009. "Single-shot Qubit Readout in Circuit Quantum Electrodynamics," *Nature Physics*, vol. 5, no. 11, pp. 791–795.

Martins, F, F. K. Malinowski, P. D. Nissen, E. Barnes, S. Fallahi, G. C. Gardner, M. J. Manfra, C. M. Marcus, and F. Kuemmeth. 2016. "Noise Suppression Using Symmetric Exchange Gates in Spin Qubits," *Physical Review Letters*, vol. 116, no. 11, 116801.

Peterer, M. J., S. J. Bader, X. Jin, F. Yan, A. Kamal, T. J. Gudmundsen, P. J. Leek, T. P. Orlando, W. D. Oliver, and S. Gustavsson. 2015. "Coherence and Decay of Higher Energy Levels of a Superconducting Transmon Qubit," *Physical Review Letters*, vol.114, no. 1, 010501.

Nayfeh, O., Simonsen, Rees, D. Naderi, S., deEscobar, A., Dinh, S., Escobar, F., Taylor, B., deAndrade, M., Berggren, S., Swanson, P., Offord, B., "Nonvolatile and Cryogenic Compatible Quantum Memory Devices", SSC Pacific Technical Report 3016, 2016

Pla, J.J.,J., Kuan Y.T,Dehollain, J.P., Lim, W.H., Morton, J.L., Zwanenburg, F.A., Jamieson, D.N., Dzurak, A.S., and Morello, A.. 2013. "High-fidelity Readout and Control of a Nuclear Spin Qubit in Silicon.." *Nature*. vol. 496, no. 7445, pp. 334–338.

Rebentrost, P., and F. K. Wilhelm. 2009. "Optimal Control of a Leaking Qubit," *Physical Review B*, vol. 79, no. 6, 060507.

REPORT DOCUMENTATION PAGE

Form Approved
OMB No. 0704-01-0188

PLEASE DO NOT RETURN YOUR FORM TO THE ABOVE ADDRESS.

1. REPORT DATE *(DD-MM-YYYY)*	**2. REPORT TYPE**	**3. DATES COVERED** *(From - To)*
September 2016	Final	

4. TITLE AND SUBTITLE

Generation of Quality Pulses for Control of Qubit/Quantum Memory Spin States: Experimental and Simulation

5a. CONTRACT NUMBER

5b. GRANT NUMBER

5c. PROGRAM ELEMENT NUMBER

6. AUTHORS

Osama Nayfeh, **SSC Pacific**
Hector Romero, Lance Lerum, **NREIP**
Mohammed Fahem, **SDSU Research Foundation**

5d. PROJECT NUMBER

5e. TASK NUMBER

5f. WORK UNIT NUMBER

7. PERFORMING ORGANIZATION NAME(S) AND ADDRESS(ES)

SSC Pacific
53560 Hull Street
San Diego, CA 92152–5001

8. PERFORMING ORGANIZATION REPORT NUMBER

TR 3046

9. SPONSORING/MONITORING AGENCY NAME(S) AND ADDRESS(ES)

SSC Pacific
In-house Laboratory Initiative for Research
53560 Hull Street
San Diego, CA 92152–5001

10. SPONSOR/MONITOR'S ACRONYM(S)

11. SPONSOR/MONITOR'S REPORT NUMBER(S)

12. DISTRIBUTION/AVAILABILITY STATEMENT

Approved for public release.

13. SUPPLEMENTARY NOTES

14. ABSTRACT

This technical report presents simulation and experimental hardware development of pulsed modulated microwave/radio frequency electronic control circuitry for control of electron/nuclear spin states of qubits/quantum memory applicable to semiconductor, superconductor, ionic and superconductor-ionic hybrid technologies. As the pulse quality and need for development of single pulses with very high quality will impact directly the coherence time of the qubit/memory, we present as an example the integration of cryogenic superconductor components including filters and amplifiers to improve the pulse quality and validate the approach. Control of qubits/quantum memory using this technology will be subject of future report.

15. SUBJECT TERMS

pulsed modulated microwave/radio frequency electronic control circuitry; control of electron/nuclear spin states; qubits/quantum memory; semiconductor, superconductor, ionic and superconductor-ionic hybrid technologies; pulse quality

16. SECURITY CLASSIFICATION OF:			**17. LIMITATION OF ABSTRACT**	**18. NUMBER OF PAGES**	**19a. NAME OF RESPONSIBLE PERSON**
a. REPORT	**b. ABSTRACT**	**c. THIS PAGE**			Osama Nayfeh
U	U	U	U	25	**19B. TELEPHONE NUMBER** *(Include area code)* (619) 553-2770

INITIAL DISTRIBUTION

84300	Library	(1)
85300	Archive/Stock	(1)
71730	O. Nayfeh	(4)

Defense Technical Information Center
Fort Belvoir, VA 22060–6218 (1)

Approved for public release.

SSC Pacific
San Diego, CA 92152-5001